Maxwell–Rankine stress functions of membrane shells and their relation to that of planar funicular gridshells

Chiang, Yu Chou

Important note
To cite this publication, please use the final published version (if applicable).
Please check the document version above.

Maxwell–Rankine stress functions of membrane shells and their relation to that of planar funicular gridshells

Yu-Chou Chiang

Faculty of Architecture and the Built Environment, Delft University of Technology, Julianalaan 134, 2628 BL Delft, The Netherlands

ARTICLE INFO

ABSTRACT

This paper investigates the correlations among 3D graphic statics, Maxwell–Rankine stress function, and Pucher's equation (the governing equation of membrane shells). When there is only vertical load, a solution of Pucher's equation can be converted into a Maxwell–Rankine stress function. The resulting stress function can be further discretized into Rankine reciprocal diagrams. The analogous membrane shell will simultaneously be discretized into a gridshell, which has planar polygonal faces and prismatoidal Rankine diagrams. A family of analytical free-edge membrane shells is also presented. Once these membrane shells are discretized, they can have co-apex pyramidal Rankine diagrams. The resulting discretized Rankine diagrams provide an intuitive way for structure designers to perceive the equilibrium of shell structures.

1. Introduction

Graphic statics is an intuitive and powerful design tool that allows a structure designer to analyze and control forces in trusses. Before the advent of computers, graphic statics was arguably the only viable means to design funicular structures (e.g. bending-moment-free trusses, arches). The resulting structures are often material efficient. To reduce the embodied greenhouse gas emissions from our construction and manufacturing industries for a more sustainable future, it is in our interest to revive and revisit such economical design methods.

Graphic statics is deeply connected with stress functions and smooth reciprocal diagrams (Maxwell, 1868, 1870). In a two-dimensional domain, the projections of a polyhedral Airy stress function and its dual figure are the Maxwell reciprocal diagrams; similarly, for a three-dimensional case, the projections of a polytopal Maxwell–Rankine stress function and its dual figure are the Rankine reciprocal diagrams (Fig. 1).

Historically, the applications of reciprocal diagrams were mainly in the discrete fashion and had been through some rises and falls. Graphic statics was popular, especially in 2D before the popularization of computers, since the available drafting tools (e.g. pen and paper) had no difficulty implementing such methods. However, with the emergence computers (ca. the 1980s), the input/output interfaces of these devices were mainly for numerical data. Therefore, matrices analysis became dominant. Meanwhile, graphical processes were relatively too computationally demanding, and thus graphic statics received less attention.

Having said that, computer graphics has been greatly improved in the latest decades. Graphics statics has regained the attention of researchers across architecture, engineering, and computer graphics (Block and Ochsendorf, 2007; Vouga et al., 2012; Konstantatou et al., 2018).

In recent years, developments in 3D visualization allows much more interesting progress in 3D graphic statics, which was not widely studied before. For instance, D'Acunto et al. (2019) developed 3D vector-based graphic statics in which the forces on a node reach equilibrium when the force vectors form a closed loop. Meanwhile using the Rankine reciprocal diagrams, Akbarzadeh et al. (2015) and Konstantatou et al. (2018) expressed a node's equilibrium by a closed polyhedron, in which an oriented facet (i.e., the normal vector and surface area of the facet) represents a force (i.e., the direction and magnitude of the force). Naturally, the net-oriented surface area of a closed polyhedron always equals zero, which promises that the net force of each node equals zero, as well.

A special type of gridshell, which has a Rankine diagram consisting of pyramids sharing the same apex point, had been shown by Akbarzadeh et al. (2015) as well as Lee et al. (2018) and McRobie et al. (2021). McRobie et al. (2021) call such a gridshell a *simple Rankine gridshell*. Considering a shell is one of the structures that can material-efficiently cover a space, the paper would like to raise two questions: *What would be the smooth counterparts of the simple Rankine gridshell?* and, *Is there a way to discretize an arbitrary membrane shell into its Rankine reciprocal diagrams?*

E-mail address: Chiang.YuChou@gmail.com.

(a)

(b)

Airy stress function $f(x, y)$

Reciprocal diagram $\phi(\xi, \eta)$

(c)

(d)

Maxwell-Rankine stress function $F(x, y, z)$

Reciprocal diagram $\Phi(\xi, \eta, \zeta)$

Smooth
(C^∞ continuity)

Discrete
(C^0 continuity)
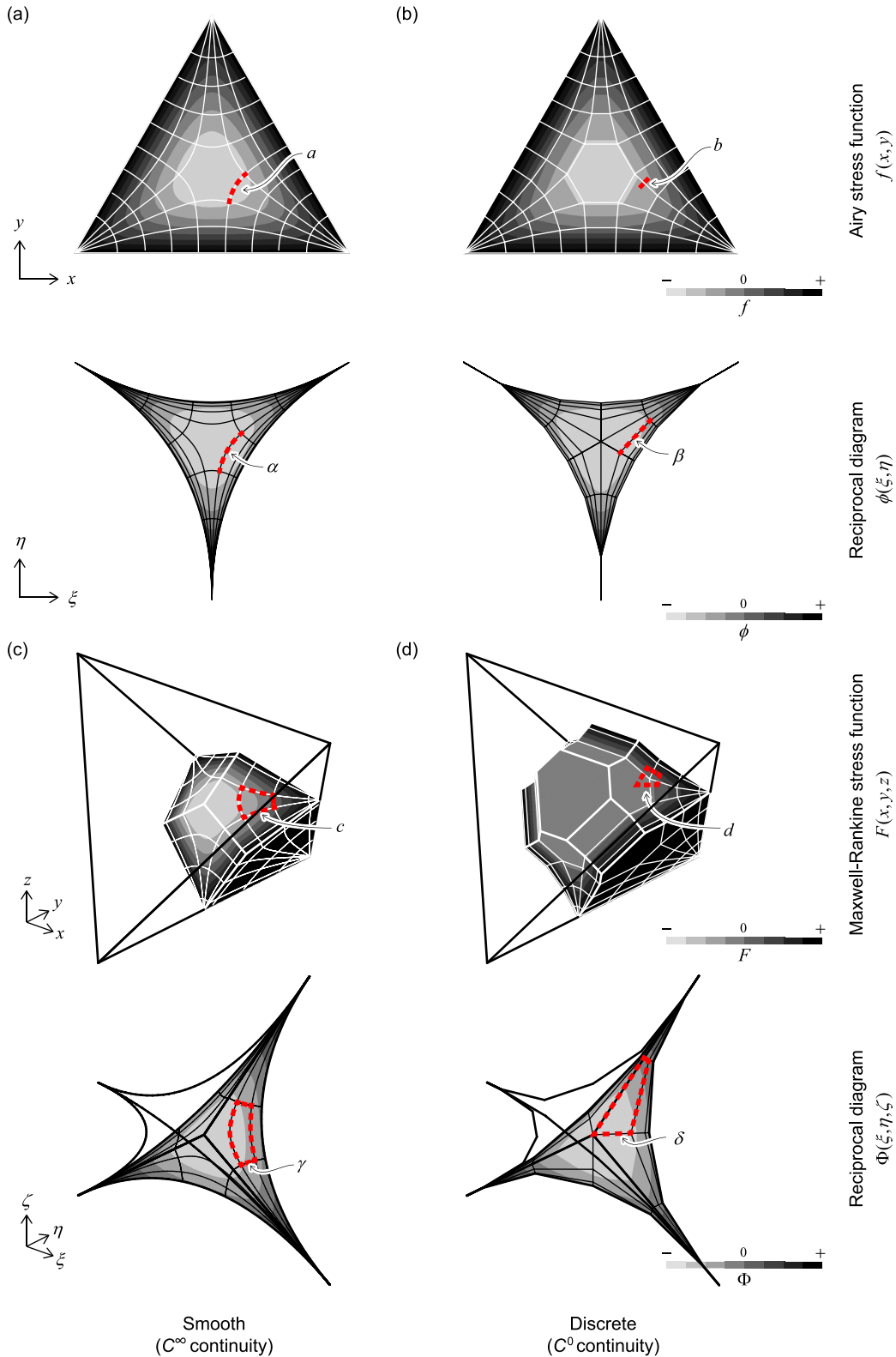
Fig. 1. Reciprocal diagrams. (a) A smooth Airy stress function $f(x, y)$ of a triangular plate stressed at the corners and its reciprocal diagram $\phi(\xi, \eta)$. The principal stress trajectories are shown as white curves on $f(x, y)$, while the corresponding trajectories are the black curves on $\phi(\xi, \eta)$. (b) The discrete counterparts of the $f(x, y)$ and $\phi(\xi, \eta)$. The stress trajectories are discretized into borders between quadrilateral patches. (c) A smooth Maxwell–Rankine stress function $F(x, y, z)$ of a tetrahedral solid stressed at the corners and its reciprocal diagram $\Phi(\xi, \eta, \zeta)$. (d) The discrete counterparts of the $F(x, y, z)$ and $\Phi(\xi, \eta, \zeta)$.

Although it had been suggested that the discretized Airy stress function and Maxwell–Rankine stress function are not limited to funicular structures (Williams and McRobie, 2016; McRobie and Williams, 2017), in this paper, we are limiting investigation to funicular frames, which can be much more material-efficient and thus preferable when designing slender structures.

Subject	Dimension		Publication scholar (year)				
Discrete reciprocal diagrams	2D	○ Varignon (1725)	○ Maxwell (1864)	○ Culmann (1866)	○	○	Cremona (1872)
	3D		○ Rankine (1864)				
Smooth reciprocal diagrams	(2+1)D				○	○	
	(3+1)D			Maxwell (1868)	○	○	Maxwell (1870)
Smooth stress function	(2+1)D	○ Airy (1863)					
	(3+1)D				○	○	

Fig. 2. Key historical publications of the related theories.

1.1. Contributions and outline

The main objective of this research is to convert a membrane shell into its Rankine reciprocal diagrams and identify what type of membrane shell can be discretized into a *simple Rankine gridshell*. With these targets in mind, the investigation has made some contributions:

- revisiting the interconnected relations among smooth stress functions, reciprocal diagrams, and graphic statics (Section 2),
- translating general solutions of Pucher's equation into smooth Maxwell–Rankine stress functions (Section 3.1),
- discretizing the smooth Maxwell–Rankine stress functions into triangular or quadrilateral prismatic polytopes (Section 3.2),
- identifying that *self-Airy membrane shells* (see Millar et al., 2021a) are the smooth counterparts of *simple Rankine gridshells* (see McRobie et al., 2021) (Section 4.1), and
- discretizing free-edge self-Airy membranes shells into co-apex pyramidal Rankine diagrams (Section 4.3).

Finally, Section 5 concludes this paper.

2. Graphic statics with reciprocal diagrams and stress functions

The theory of graphic statics intertwines with those of stress functions and reciprocal diagrams. The development of these theories also tangled (Fig. 2). The development of 2D graphic statics can be traced back to Varignon (1725), then Maxwell (1864), Culmann (1866), and Cremona (1875) carried on the investigation. Instead of using a closed polygon to express the equilibrium of a node in a 2D structure, Rankine (1864) proposed a method of using a closed polyhedron to express the equilibrium of a node in a 3D structure. In the same year, Airy (1863) proposed his seminal theory on extracting an auto-equilibrium stress tensor field from a single scalar function, which is called the Airy stress function in present days. More importantly, Maxwell (1868) extended the notions of discrete reciprocal diagrams to smooth scalar functions and identified that the reciprocal diagram of a smooth 2D function would yield the same mechanical interpretation as of the Airy stress functions. Eventually, Maxwell (1870) unified all related theories and pointed out that when a smooth Airy stress function is discretized into a polyhedral one, the reciprocal result is identical to its Maxwell reciprocal diagram; when a smooth Maxwell–Rankine stress function is discretized into a polytopal one, the reciprocal result is identical to its Rankine reciprocal diagram.

Historically, the discrete reciprocal diagrams were proposed earlier than the stress functions and smooth reciprocal diagrams. However, we can discuss the notions backward, since the definitions of stress functions and smooth reciprocal diagrams are more general than the discrete counterparts.

2.1. Smooth reciprocal diagrams

Maxwell (1868, 1870) stated the existence of a mutual mapping between two smooth reciprocal multivariable functions. Let the two

functions be $F(x, y, z)$ and $\Phi(\xi, \eta, \zeta)$, and the mapping is provided by

$$\xi = \partial_x F, \ \eta = \partial_y F, \ \zeta = \partial_z F, \ \Phi = x\,\partial_x F + y\,\partial_y F + z\,\partial_z F - F, \tag{1a}$$

$$x = \partial_\xi \Phi, \ y = \partial_\eta \Phi, \ z = \partial_\zeta \Phi, \ F = \xi\,\partial_\xi \Phi + \eta\,\partial_\eta \Phi + \zeta\,\partial_\zeta \Phi - \Phi, \tag{1b}$$

in which $\partial_x = \partial/\partial x$ is Euler's notation for the derivatives. When the functions are continuously differentiable, a point on $F(x, y, z)$ maps to a point on $\Phi(\xi, \eta, \zeta)$ and vice versa. Maxwell suggested an interesting mechanical feature of the reciprocal diagrams. When a surface element in the (x, y, z) domain (e.g. area c in Fig. 1c) has the same resultant force as a uniform normal stress P_0 acting on the corresponding element in the (ξ, η, ζ) domain (e.g. area γ in Fig. 1c), such a stress tensor field will automatically satisfy the equilibrium conditions

$$\sum_i \partial_i \sigma_{ij} = 0, \tag{2}$$

in which $i, j \in \{x, y, z\}$. The stress tensor field in (x, y, z) can be expressed as

$$\sigma_{xx} = P_0\,[\partial_{yy} F \cdot \partial_{zz} F - (\partial_{yz} F)^2], \tag{3a}$$

$$\sigma_{yy} = P_0\,[\partial_{zz} F \cdot \partial_{xx} F - (\partial_{zx} F)^2], \tag{3b}$$

$$\sigma_{zz} = P_0\,[\partial_{xx} F \cdot \partial_{yy} F - (\partial_{xy} F)^2], \tag{3c}$$

$$\sigma_{xy} = P_0\,[\partial_{yz} F \cdot \partial_{zx} F - \partial_{zz} F \cdot \partial_{xy} F], \tag{3d}$$

$$\sigma_{xz} = P_0\,[\partial_{xy} F \cdot \partial_{yz} F - \partial_{yy} F \cdot \partial_{zx} F], \tag{3e}$$

$$\sigma_{yz} = P_0\,[\partial_{zx} F \cdot \partial_{xy} F - \partial_{xx} F \cdot \partial_{yz} F]. \tag{3f}$$

The stress function $F(x, y, z)$ is called the Maxwell–Rankine stress function (McRobie and Williams, 2017).

In a two dimensional case, the reciprocal relations between the functions $f(x, y)$ and $\phi(\xi, \eta)$ turn into

$$\xi = \partial_x f, \quad \eta = \partial_y f, \quad \phi = x\,\partial_x f + y\,\partial_y f - f, \tag{4a}$$

$$x = \partial_\xi \phi, \quad y = \partial_\eta \phi, \quad f = \xi\,\partial_\xi \phi + \eta\,\partial_\eta \phi - \phi. \tag{4b}$$

Similarly, when an element of a line segment in the (x, y) domain (e.g. segmen a in Fig. 1a) has the same resultant force as a uniform normal stress p_0 acting on the corresponding element of the line segment in the (ξ, η) domain (e.g. segment α in Fig. 1a), such a stress tensor field will also automatically satisfy equilibrium conditions (2) when $i, j \in \{x, y\}$. The 2D stress tensor field in (x, y) can be expressed as

$$\sigma_{xx} = p_0\,\partial_{yy} f, \tag{5a}$$

$$\sigma_{yy} = p_0\,\partial_{xx} f, \tag{5b}$$

$$\sigma_{xy} = -p_0\,\partial_{xy} f, \tag{5c}$$

The stress function $f(x, y)$ is generally called the Airy stress function.

To be noted, in this paper, we use capital F and Φ for the reciprocal diagrams of 3D Maxwell–Rankine stress functions and use lowercase f and ϕ for the reciprocal diagrams of 2D Airy stress functions.
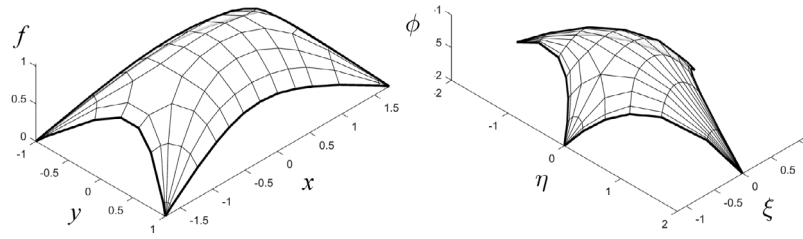
Fig. 3. Graphs of a polyhedral Airy stress function $f(x,y)$ and its Maxwell reciprocal diagram $\phi(\xi,\eta)$.

2.2. Discrete reciprocal diagrams

When the stress functions are discretized, they are not continuously differentiable anymore. A discretized Airy stress function consists of a series of polygonal patches, in any of which the gradients $\partial_x f$ and $\partial_y f$ are constants. One may graph such a 2D discretized stress function in a $(2+1)$D space as a polyhedral surface $\{x, y, f(x,y)\}$. All points on a planar facet of such a polyhedral surface correspond to a single point on the reciprocal surface $\{\xi, \eta, \phi(\xi, \eta)\}$. Meanwhile, a summit surrounded by n facets corresponds to the polygon formed by the n corresponding points (Fig. 3).

Regarding the 3D discretized Maxwell–Rankine stress function, all the geometry elements receive one more dimension. A discretized Maxwell–Rankine stress function consists of a series of polyhedral patches, in any of which the gradients $\partial_x F$, $\partial_y F$, and $\partial_z F$ are constants. Should someone graph the 3D discretized stress function, the result is in a $(3+1)$D space as a polytopal hyper-surface $\{x, y, z, F(x, y, z)\}$. All points in a polyhedral cell of such a polytopal hyper-surface correspond to a single point on the reciprocal hyper-surface $\{\xi, \eta, \zeta, \Phi(\xi, \eta, \zeta)\}$. Meanwhile, a summit surrounded by n polyhedral cells corresponds to the polyhedron formed by the n corresponding points.

It would be quite challenging to visualize such polytopal hyper-surfaces, but visualizing the projections of the borders would be much easier. As we can project the borders between polygonal patches of the polyhedral Airy stress function $f(x,y)$ onto a 2D plane (Fig. 1b), we can project the border between polyhedral patches of the polytopal Maxwell–Rankine stress function $F(x, y, z)$ into a 3D space (Fig. 1d). When a smooth stress function is discretized along the trajectories of principal stresses, the result can be a quadrilateral mesh (Fig. 1b) or a hexahedral mesh (Fig. 1d).

This section has revisited the smooth and discrete reciprocal diagrams. The notions from $(2+1)$D polyhedral Airy stress functions are extended to $(3+1)$D polytopal Maxwell–Rankine stress functions. In the following sections, the discussion will focus on smooth and discrete Maxwell–Rankine stress functions and their diagrams.

3. Pucher's equation and Maxwell–Rankine stress function for general membrane shells

Pucher's equation governs the 3D equilibrium of membrane shells, which might arguably be the most simple yet expressive 3D structures. However, to the best of the author's knowledge, there is no direct way to convert a solution of Pucher's equation into a Maxwell–Rankine stress function. This section is going to provide such a conversion and further discretize the stress functions into polytopal ones.

3.1. Smooth Maxwell–Rankine stress functions of membrane shells

Pucher's equation relates the 2D stress resultant (represented by the Airy stress function), the shape function, and the external loads. In the absences of horizontal loads, the governing differential equation – Pucher's equation – is expressed as (Timoshenko and Woinowsky-Krieger, 1959, p. 461)

$$\partial_{yy} f \cdot \partial_{xx} s - 2\partial_{xy} f \cdot \partial_{xy} s + \partial_{xx} f \cdot \partial_{yy} s = -p_z, \tag{6}$$

where $f(x,y)$ is the Airy stress function for the horizontal stress resultants, $s(x,y)$ is the shape of the shell, and p_z is the vertical load (per unit horizontal area). This single scalar equation can adequately express the equilibrium in all x-, y-, and z-directions.

For a pair of the Airy stress function $f(x,y)$ and shape function $s(x,y)$, the corresponding Maxwell–Rankine stress function $F(x,y,z)$ can be expressed as

$$F(x,y,z) = \alpha f(x,y) + \begin{cases} -\beta[s(x,y) - z], & z > s(x,y), \\ \beta[s(x,y) - z], & z \le s(x,y), \end{cases} \tag{7}$$

where α and β are constants. According to Eq. (3), at places above or below the membrane shell ($z \ne s(x,y)$), one can easily derive that stress function $F(x,y,z)$ in (7) yields five zero stress components: $\sigma_{xx} = \sigma_{yy} = \sigma_{xy} = \sigma_{yz} = \sigma_{yz} = 0$. The only non-zero stress component, σ_{zz}, takes forms of

$$\frac{\sigma_{zz}}{P_0} = \begin{cases} \alpha^2 \partial_{xx} f \cdot \partial_{yy} f - \alpha\beta(\partial_{xx} f \cdot \partial_{yy} s + \partial_{xx} s \cdot \partial_{yy} f) \\ \qquad + \beta^2 \partial_{xx} s \cdot \partial_{yy} s - \alpha^2 (\partial_{xy} f)^2 \\ \qquad + 2\alpha\beta \partial_{xy} f \cdot \partial_{xy} s - \beta^2 (\partial_{xy} s)^2, & z > s(x,y), \\ \alpha^2 \partial_{xx} f \cdot \partial_{yy} f + \alpha\beta(\partial_{xx} f \cdot \partial_{yy} s + \partial_{xx} s \cdot \partial_{yy} f) \\ \qquad + \beta^2 \partial_{xx} s \cdot \partial_{yy} s - \alpha^2 (\partial_{xy} f)^2 \\ \qquad - 2\alpha\beta \partial_{xy} f \cdot \partial_{xy} s - \beta^2 (\partial_{xy} s)^2, & z < s(x,y). \end{cases} \tag{8}$$

The difference in the vertical stress σ_{zz} above and below the surface $z = s(x,y)$ yields

$$\sigma_{zz}\big|_{z > s(x,y)} - \sigma_{zz}\big|_{z < s(x,y)} = -2\alpha\beta P_0 (\partial_{xx} f \cdot \partial_{yy} s + \partial_{xx} s \cdot \partial_{yy} f)$$
$$+ 4\alpha\beta P_0 \partial_{xy} f \cdot \partial_{xy} s, \tag{9}$$

$$= 2\alpha\beta P_0 p_z, \tag{10}$$

in which the right-hand side of Eq. (9) has the same terms as the left-hand side of Pucher's equation (6), therefore we can arrive at Eq. (10). Once $\alpha\beta P_0 = 1/2$, the expression (7) can sufficiently convert a solution of Pucher's equation into a Maxwell–Rankine stress function.

3.2. Polytopal Maxwell–Rankine stress functions of gridshells

Since the 1980s, scholars have discretized the shape functions and the Airy stress functions of membrane shells into triangular meshes (Hedgűs, 1984). The triangular polyhedral Airy stress functions are flexible to approximate arbitrary 2D stress field or the horizontal stress resultant field of shells, and thus they are often used in computational applications (Fraternali et al., 2002; Vouga et al., 2012; Pellis and Pottmann, 2018).

Instead of discretizing Airy stress functions into polygonal patches, this paper discretized the Maxwell–Rankine stress functions (7) of membrane shells into prismatic cells. The corresponding Rankine reciprocal diagrams will consist of frustums (Figs. 4 and 5).

3.2.1. Triangular discretization

To discretize the stress function (7) into triangular prismatic cells is rather straightforward.

One can start from a 2D triangular mesh, which has n faces f_i, $i \in \{1, \dots, n\}$, formed by vertices (x_j^i, y_j^i), $j \in \{1, 2, 3\}$. Subsequently,
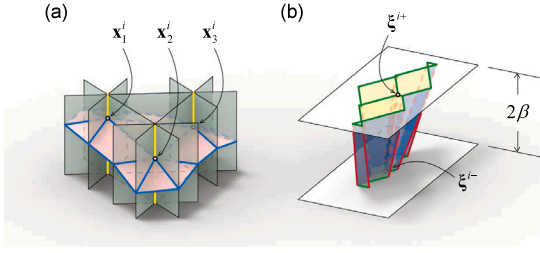
Fig. 4. A triangular gridshell (a) and its Rankine diagrams (b). The vertical loads (yellow lines) and the compression forces (blue lines) of the grids shells correspond to parallel faces (yellow) and lateral faces (blue) of the prismatoids. Prismatic cells above and below the triangle $\mathbf{x}_1^i\mathbf{x}_2^i\mathbf{x}_3^i$ correspond to vertices ξ^{i+} and ξ^{i-}.

Fig. 5. A non-triangular gridshell (a) and its Rankine diagrams (b). The vertical loads (yellow lines) and the compression forces (blue lines) of the grids shells correspond to parallel faces (yellow) and lateral faces (blue) of the prismatoids. Prismatic cells above and bellow the hexagon $\mathbf{x}_1^i\mathbf{x}_2^i\dots\mathbf{x}_6^i$ correspond to vertices ξ^{i+} and ξ^{i-}, which connect 6 edges in the horizontal planes.

one can project the triangular faces onto the surface $s(x,y)$ and beyond. Each resulting triangular prism should have 3 edges intersecting the surface at 3 points $\mathbf{x}_j^i = (x_j^i, y_j^i, s_j^i)$, in which $s_j^i = s(x_j^i, y_j^i)$. The points can further define a triangle f_i' that cuts the prism into two segments: one above the triangle and the other one below. Let triangle f_i' seal the bottom of the upper prismatic segment and cap the lower prismatic segment (Fig. 4).

So far, the borders between the cells are defined. The remaining task is to evaluate the three gradients ξ, η, ζ; and one value Φ for each cell. Then, we can complete the Rankine reciprocal diagrams.

We can start the evaluation from the upper cells, where the gradient $\zeta = \partial_z F$ is constantly equal to $+\beta$ according to Eq. (7). The ith upper cell has three vertices on the surface $s(x,y)$. The values F_j^i of the stress function at these vertices shall be provided by

$$F_j^i = F(x_j^i, y_j^i, s_j^i) = \alpha f_j^i = \alpha f(x_j^i, y_j^i). \tag{11}$$

These values can sufficiently determine the two remaining gradients ξ^{i+}, η^{i+}; and one value Φ^{i+} in the cell:

$$\begin{bmatrix} \xi^{i+} \\ \eta^{i+} \\ \Phi^{i+} \end{bmatrix} = \begin{bmatrix} x_1^i & y_1^i & -1 \\ x_2^i & y_2^i & -1 \\ x_3^i & y_3^i & -1 \end{bmatrix}^{-1} \left(\alpha \begin{bmatrix} f_1^i \\ f_2^i \\ f_3^i \end{bmatrix} - \beta \begin{bmatrix} s_1^i \\ s_2^i \\ s_3^i \end{bmatrix} \right). \tag{12}$$

Similarly, for the lower cells, we have $\zeta^{i-} = -\beta$ and

$$\begin{bmatrix} \xi^{i-} \\ \eta^{i-} \\ \Phi^{i-} \end{bmatrix} = \begin{bmatrix} x_1^i & y_1^i & -1 \\ x_2^i & y_2^i & -1 \\ x_3^i & y_3^i & -1 \end{bmatrix}^{-1} \left(\alpha \begin{bmatrix} f_1^i \\ f_2^i \\ f_3^i \end{bmatrix} + \beta \begin{bmatrix} s_1^i \\ s_2^i \\ s_3^i \end{bmatrix} \right). \tag{13}$$

Thus, the polytopal Maxwell–Rankine stress function defined by vertices $(x_j^i, y_j^i, s_j^i, F_j^i)$ is corresponding to another polytopal hyper-surface defined by vertices $\xi^{i+} = (\xi^{i+}, \eta^{i+}, +\beta, \Phi^{i+})$ and $\xi^{i-} = (\xi^{i-}, \eta^{i-}, -\beta, \Phi^{i-})$.

Fig. 4 shows a simple example of a triangular gridshell. For a more realistic structure, the numerical method of radial basis functions (Chiang and Borgart, 2022) is used to generate a pair of smooth Airy stress function $f(x,y)$ and shape function $s(x,y)$ subjected to a uniform unit vertical load $p_z = -1$. The result of discretization is displayed in Fig. 7a. Since these examples are compression-dominated shells, the coefficients are set as $\alpha = -1$, $\beta = 1/2$, and $P_0 = -1$.

3.2.2. Quadrilateral discretization

Discretizing a smooth Maxwell–Rankine stress function (7) into non-triangular prismatic cells is not so trivial. Adding one more vertex into Eq. (12) or (13), we will have an overdetermined system. However, we can treat the fourth vertex as unknown and list conditions to locate it.

For a pair of quadrilateral prismatic cells, let us assume that the first three vertices (x_j, y_j, s_j, F_j) of the middle quadrilateral are known. Then, we can derive the parameters $\xi^+, \eta^+, \Phi^+, \xi^-, \eta^-$, and Φ^- of the upper and lower cells by Eqs. (12) and (13). The fourth vertex
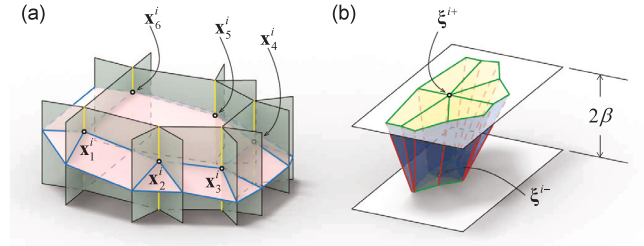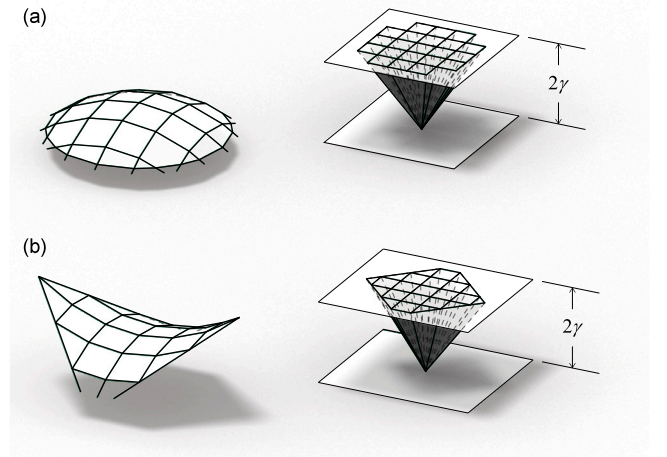
Fig. 6. Rankine diagrams of self-Airy gridshells. (a) $s = x^2 + y^2$. (b) $s = 2xy$. (The lines of vertical loads and the walls between prismatic cells are omitted for visual clarity).

(x_4, y_4, z_4, F_4) shall be located at the intersection of four hyper-surfaces:

$$\begin{cases} F_4 = \xi^+ x_4 + \eta^+ y_4 + \beta z_4 - \Phi^+, \\ F_4 = \xi^- x_4 + \eta^- y_4 - \beta z_4 - \Phi^-, \\ F_4 = F(x_4, y_4, z_4), \\ z_4 = s(x_4, y_4). \end{cases} \tag{14}$$

By Eq. (14), we can locate the fourth vertex when the other three vertices are given. In regions that all vertices have the same valence 6 (1 to $z = \infty$, 1 to $z = -\infty$, and the other 4 to neighborhood vertices) and all prismatic cells are quadrilateral, we can derive quadrilateral prismatic cells with m-by-n 4D vertices when $(m+n-1)$ 2D vertices are provided. A strategy of arranging the starting vertices based on *conjugate curve networks* (Liu et al., 2006) for a given membrane shell is briefly discussed in Appendix. This discretization method can also be used to re-mesh the results from other mesh-based numerical solutions (Block and Ochsendorf, 2007; Vouga et al., 2012; de Goes et al., 2013; Pellis and Pottmann, 2018).

Occasionally, the discretization requires some singular vertices (valance other than 6) or singular prismatic cells (non-quadrilateral prisms). For further discussion on the singularity, readers are referred to Zadravec et al. (2010) and Li et al. (2012), or (Douthe et al., 2017).

Fig. 7b shows a discrete stress function of a quadrilateral gridshell. The closeups of the singular hexagonal prismatic cells are shown in Fig. 5.
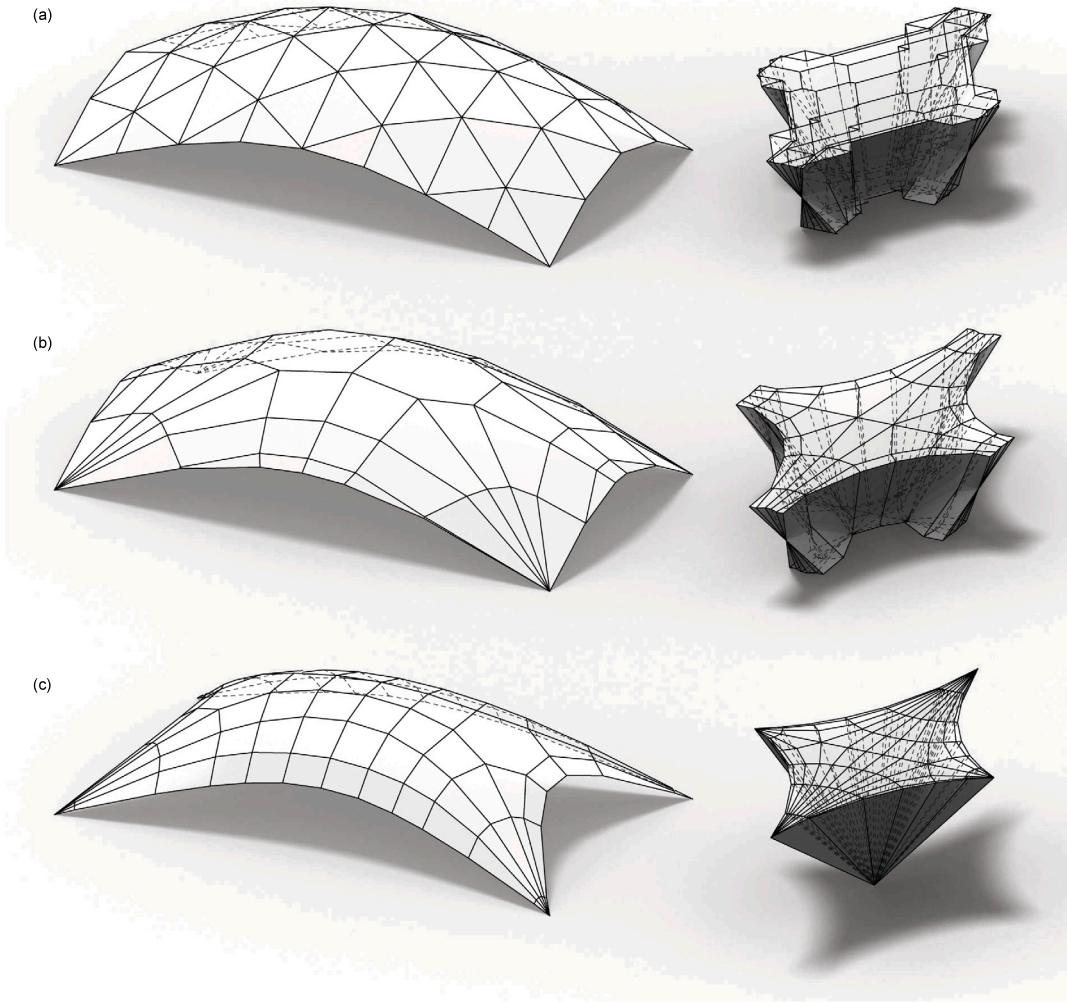
Fig. 7. Planar funicular gridshells and their Rankine diagrams. (a) A triangular gridshell. (b). A quadrilateral gridshell. Although discretized into different patterns, both (a) and (b) are based on a common membrane shell. (c) A self-Airy gridshell, which has distinctly curved free edges tangent to planes. (Vertical lines to $z = \pm\infty$ are excluded for visual clarity).

4. Self-Airy shells

This section further investigates what type of membrane shell can be discretized into a *simple Rankine gridshell* (McRobie et al., 2021), which has a Rankine diagram consisting of co-apex pyramids. Some non-trivial analytical instances are provided (Section 4.2), which are later discretized into quadrilateral Rankine diagrams (Section 4.3).

4.1. Simple Rankine gridshells and self-Airy shells

A shell's Maxwell–Rankine stress function (7) has upper and lower parts that read $F = \alpha f \mp \beta s \pm \beta z$. If $\alpha f = \pm \beta s$, which means the Airy stress function $f(x, y)$ is linearly proportional to the shape function $s(x, y)$, the stress function can be greatly simplified. Let $f(x, y) = 2\delta\gamma^2 s(x, y)$, in which $\delta = \pm 1$ and $\gamma \geq 0$. When $\alpha = -\delta/(2\gamma)$ and $\beta = \gamma$, the Maxwell–Rankine stress function (7) turns into

$$F(x, y, z) = \begin{cases} -2\gamma s(x, y) + \gamma z, & z > s(x, y), \\ -\gamma z, & z \leq s(x, y). \end{cases} \quad (15)$$

In this case, any point below $z = s(x, y)$ corresponds to a common point $(0, 0, -\gamma)$ in the (ξ, η, ζ) domain. This is the main feature of *simple Rankine gridshells*. Thus, we can proclaim that the smooth counterparts of *simple Rankine gridshells* shall be the membrane shells that have Airy stress functions linearly proportional to their shapes. Furthermore,

we call these special instances *self-Airy membrane shells*, extending the terminology *self-Airy gridshells* used by Millar et al. (2021b) on the discrete version.

For self-Airy membrane shells that have $f(x, y) = 2\delta\gamma^2 s(x, y)$ ($\delta = \pm 1$ and $\gamma \geq 0$), the Pucher's equation (6) degenerates into

$$4\delta\gamma^2 [\partial_{xx} s \cdot \partial_{yy} s - (\partial_{xy} s)^2] = -p_z. \quad (16)$$

When the load p_z is constant, the solutions to this equation can be as simple as paraboloids such as the elliptic one $s = x^2 + y^2$ and the hyperbolic one $s = 2xy$. These simple solutions can be easily discretized into quadrilateral gridshells (Fig. 6).

For a more interesting example, the numerical method of radial basis functions (Chiang and Borgart, 2022; Chiang, 2022) is used again. Fig. 7c shows a discretized result, which is a points-supported shell with free edges. At the free edges, the self-Airy membrane shell has to comply with all conventional free edge conditions imposing on the Airy stress function:

$$\partial_{nn} s = 0, \qquad \partial_{nt} s = 0, \quad (17)$$

where n and t denote the normal and tangential directions at the free edges. These two conditions require free edges have tangent planes (Csonka, 1987; Miki et al., 2015). Having two boundary conditions around all the edges and a second-order governing equation, finding the form of a point-supported self-Airy membrane has to be
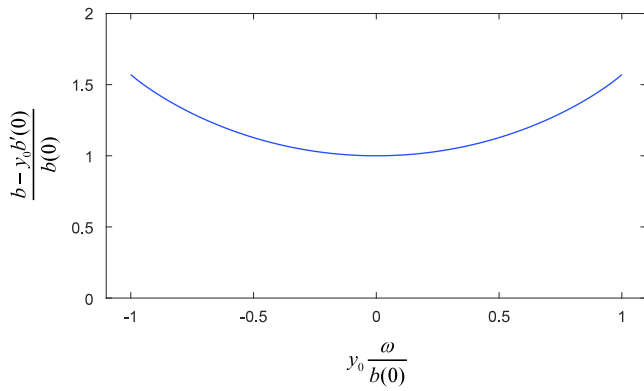
Fig. 8. The general solution of the $b - y_0$ curve.

formulated as a free boundary problem (Chiang, 2022). The shapes of the curved free-edges are not designed but are part of the solution of the free boundary problem.

4.2. Analytical self-Airy shells with free edges

Chiang (2022) provided a set of analytical solutions of self-Airy membrane shells that have free edges. Here, we briefly revisit the analytical solutions. The solutions have a standard cross-section $s_0 = b(y_0)$ sweeping along the x-axis and gradually scaled by function $a(x)$, which means

$$s(x, y) = a(x) \cdot b(y_0), \tag{18}$$

where $y_0 = y/a(x)$. Subsequently, one can derive the second derivatives as

$$\partial_{xx} s = a'' b - a'' y_0 b' + \frac{a'^2}{a} y_0^2 b'',$$

$$\partial_{yy} s = \frac{1}{a} b'',$$

$$\partial_{xy} s = -\frac{a'}{a} y_0 b''.$$

These expressions turn Eq. (16) into

$$\frac{a''}{a} b'' (b - y_0 b') = \frac{-p_z}{4 \delta \gamma^2}. \tag{19}$$

Since p_z shall be a non-zero constant, the equation can be satisfied whenever both a''/a and $b''(b - y_0 b')$ are non-zero constants. The solutions of $a(x)$ and $b(x)$ can be expressed as

$$a(x) = e^{\lambda x}, \qquad \cosh(\lambda x), \quad \text{or} \quad \cos(\lambda x), \tag{20}$$

$$b(y_0) = C_0 \left[\sqrt{1 - \left(y_0 \frac{\omega}{C_0} \right)^2} + y_0 \frac{\omega}{C_0} \arcsin \left(y_0 \frac{\omega}{C_0} \right) \right] + C_1 y_0, \tag{21}$$

where $\omega^2 = |b''(b - y_0 b')|$ is a constant related to overall curvature and $C_0 = b(0)$ and $C_1 = b'(0)$ are constants of integration. Then, these $a(x)$ and $b(y_0)$ make Eq. (19) become $\lambda^2 \omega^2 = -p_z/(4 \delta \gamma^2)$. The general solution of $b(y_0)$ is plotted in Fig. 8.

4.3. Polytopal Maxwell–Rankine stress functions of self-Airy gridshells

We can further convert the aforementioned solutions into smooth Maxwell–Rankine stress functions through Eq. (15), and discretize the results into polytopal ones. Quadrilateral discretization is preferable since its Rankine diagram is more legible than one from triangular discretization (Fig. 7a & b).

For a general shell, we can use Eqs. (14) to locate the fourth vertex of a quadrilateral prismatic cell when the other 3 vertices are

provided. For a self-Airy shell, however, Eqs. (14) cannot determine a unique fourth vertex. Since self-Airy shells have the Airy stress function linearly proportional to the shape functions, the last two equations in (14) become linearly dependent.

This paper uses *isotropic-circular mesh* (Pottmann and Liu, 2007) instead. As a result, each prismatic cell has vertices on the lateral surface of a vertical cylinder. This condition provides a means to uniquely determine the fourth vertex of a prismatic cell. Furthermore, the resulting edges will form the *isotropic*-principal-curvature lines of the surface $z = s(x, y)$. For the definition and detailed features of *isotropic-circular mesh*, readers are referred to the paper by Pottmann and Liu (2007).

To locate the fourth vertex of a quadrilateral prismatic cell for such an *isotropic*-circular mesh, one shall find a replacement of either the third or the fourth equation in (14). Let (x_c, y_c) and r denote the center axis and radius of the circumscribed vertical cylinder determined by the first there vertices $(x_i, y_i), i \in \{1, 2, 3\}$. Subsequently, one can revise the third equation in (14), and locate the fourth vertex (x_4, y_4, z_4, F_4) at the intersection of four hyper-surfaces:

$$\begin{cases} F_4 = \xi^+ x_4 + \eta^+ y_4 + \gamma z_4 - \Phi^+, \\ F_4 = -\gamma z_4, \\ r^2 = (x_4 - x_c)^2 + (y_4 - y_c)^2, \\ z_4 = s(x_4, y_4). \end{cases} \tag{22}$$

The second equation in (22) is also simplified due to the expression (15).

Eqs. (22) can help us to discretize the smooth stress functions into quadrilateral prismatic cells and corresponding Rankine diagrams. The results are illustrated in Figs. 7c and 9.

5. Conclusions

This paper has presented a method to convert solutions of membrane shells to Maxwell–Rankine stress functions and further discretize them into Rankine diagrams, which are powerful means to graphically show how forces flow in 3D space. This method has been tested to discretize smooth numerical solutions from the method of radial basis functions and can potentially be applied to re-mesh dense triangular thrust networks into planar-quadrilateral funicular gridshells.

Self-Airy membrane shells are identified to be the special cases that allow co-apex pyramidal Rankine diagrams. A family of analytical self-Airy membranes with free edges is also provided and discretized into Rankine diagrams.

Further valuable investigations on Rankine diagrams of shells would consider horizontal loads and bending resistances of the shell. Regarding the self-Airy membrane shells, their free edge conditions and numerical form-finding methods also deserve more detailed discussion and investigation.

Declaration of competing interest

The authors declare that they have no known competing financial interests or personal relationships that could have appeared to influence the work reported in this paper.

Acknowledgments

(a)

(b)

(c)
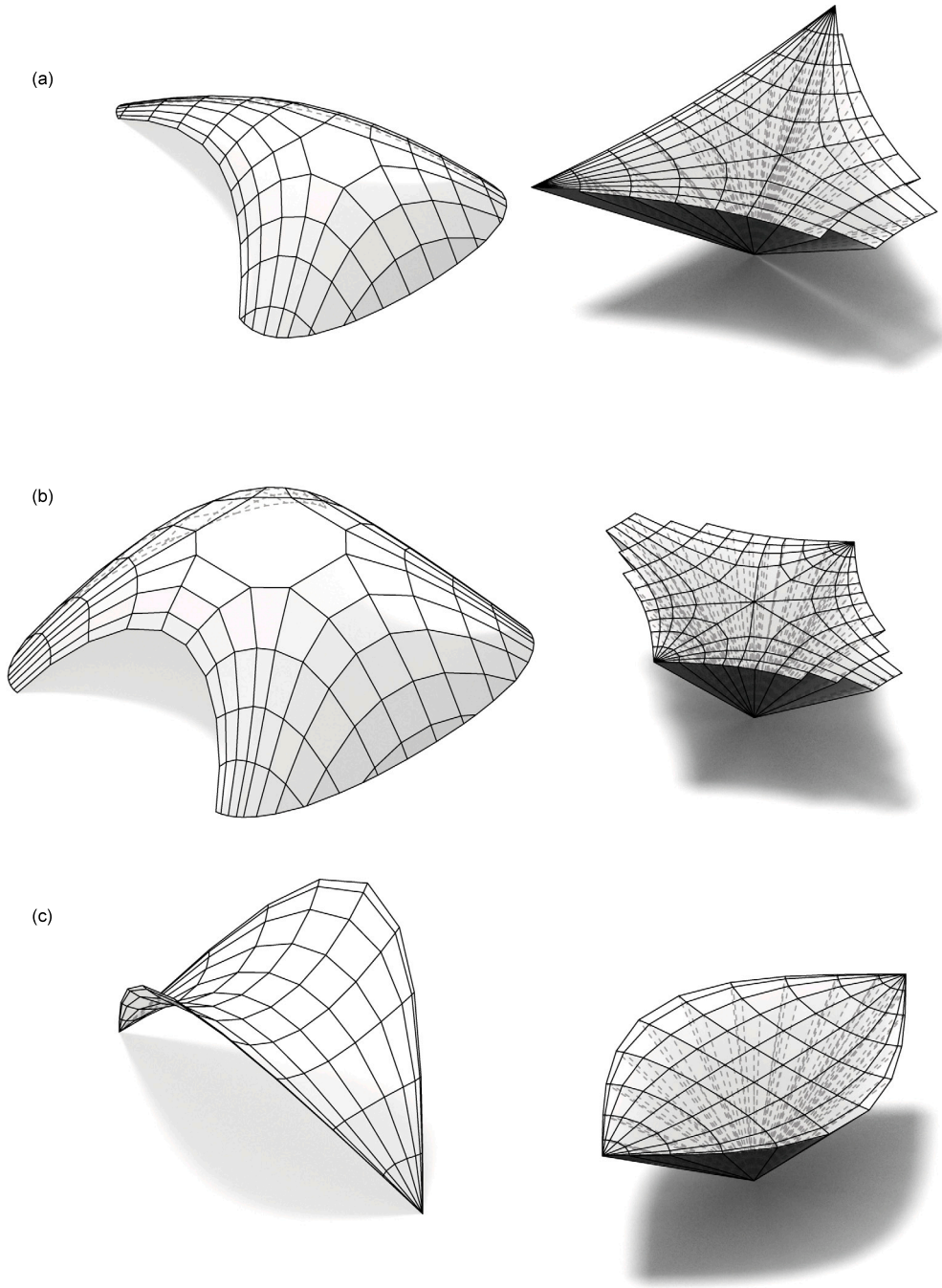
Fig. 9. Discretized analytical self-Airy shells and their Rankine diagrams. All self-Airy shells are drawn with the same $b - y_0$ curve when $b(0) = 1$ and $b'(0) = 0$. The $a(x)$ curves are $-\exp(x)$, $-\cosh(x)$, and $\cos(x)$ in panels (a), (b), and (c) respectively.

Appendix. Conjugate curve networks

To discretize a smooth two-variable scalar function $z = g(x, y)$ into a group of C^0 continuous planar quadrilateral patches, one can make use of conjugate curve networks (Liu et al., 2006; Zadravec et al., 2010; Millar et al., 2021a), which consist of two families of curves that have unit projected tangent vectors $\mathbf{t}_1 = [\cos\theta_1 \ \sin\theta_1]^T$ and $\mathbf{t}_2 = [\cos\theta_2 \ \sin\theta_2]^T$ satisfy

$$\mathbf{t}_1^T \mathbf{H}_g \mathbf{t}_2 = 0,$$

where $\mathbf{H}_g$ denotes the Hessian matrix of function $g(x, y)$. Such a conjugate curve network can guide the arrangement of quadrilateral patches.

For the task of discretizing stress function (7) into quadrilateral prismatic cells, the projected vectors $\mathbf{t}_1$ and $\mathbf{t}_2$ shall satisfy two conditions:

$$\begin{cases} \mathbf{t}_1^T \mathbf{H}_{\alpha f - \beta s} \mathbf{t}_2 = 0, \\ \mathbf{t}_1^T \mathbf{H}_{\alpha f + \beta s} \mathbf{t}_2 = 0. \end{cases}$$

These two conditions can uniquely determine the set of vectors $\mathbf{t}_1$ and $\mathbf{t}_2$. The solution exists when there is a non-hyperbolic linear combination of $\mathbf{H}_f$ and $\mathbf{H}_s$:

$$\det[a\mathbf{H}_f + (1 - a)\mathbf{H}_s] \geq 0, \qquad a \in \mathbb{R}.$$

Therefore, when the membrane shell is in pure tension or pure compression ($det(\mathbf{H}_f) > 0$), the solution of $\mathbf{t}_1$, $\mathbf{t}_2$ exists everywhere. The vector

fields $\mathbf{t}_1(x, y)$ and $\mathbf{t}_2(x, y)$ can provide the basic guide for the polytopal discretization.

References

Airy, G.B., 1863. On the strains in the interior of beams. Philos. Trans. R. Soc. Lond. 153, 49–79.

Akbarzadeh, M., Van Mele, T., Block, P., 2015. On the equilibrium of funicular polyhedral frames and convex polyhedral force diagrams. Comput. Aided Des. 63, 118–128. http://dx.doi.org/10.1016/j.cad.2015.01.006.

Block, P., Ochsendorf, J., 2007. Thrust network analysis: A new methodology for three-dimensional equilibrium. J. Int. Assoc. Shell Spatial Struct. 48 (155), 167–173.

Chiang, Y.-C., 2022. Design and Fabrication of Shell Structures: Aided by Radial Basis Functions and Reconfigurable Mechanisms (Ph.D. thesis). Delft University of Technology, http://dx.doi.org/10.7480/abe.2022.03.

Chiang, Y.-C., Borgart, A., 2022. A form-finding method for membrane shells with radial basis functions. Eng. Struct. 251, 113514. http://dx.doi.org/10.1016/j.engstruct.2021.113514.

Cremona, L., 1875. Le Figure Reciproche Nella Statica Grafica. Tipografia di G. Bernardoni, Milano.

Csonka, P., 1987. Theory and Practice of Membrane Shells. VDI Verlag, Düsseldorf.

Culmann, C., 1866. Die Graphische Statik. Meyer & Zeller, Zürich.

D'Acunto, P., Jasienski, J.P., Ohlbrock, P.O., Fivet, C., Schwartz, J., Zastavni, D., 2019. Vector-based 3D graphic statics: A framework for the design of spatial structures based on the relation between form and forces. Int. J. Solids Struct. 167, 58–70. http://dx.doi.org/10.1016/j.ijsolstr.2019.02.008.

Douthe, C., Mesnil, R., Orts, H., Baverel, O., 2017. Isoradial meshes: Covering elastic gridshells with planar facets. Autom. Constr. 83 (July 2016), 222–236. http://dx.doi.org/10.1016/j.autcon.2017.08.015.

Fraternali, F., Angelillo, M., Fortunato, A., 2002. A lumped stress method for plane elastic problems and the discrete-continuum approximation. Int. J. Solids Struct. 39 (25), 6211–6240. http://dx.doi.org/10.1016/S0020-7683(02)00472-9.

de Goes, F., Alliez, P., Owhadi, H., Desbrun, M., 2013. On the equilibrium of simplicial masonry structures. ACM Trans. Graph. 32 (4), http://dx.doi.org/10.1145/2461912.2461932.

Hedgűs, I., 1984. Stress function of single-layer reticulated shells and its relation to that of continuous membrane shells. Acta Techn. Acad. Sci. Hungaricae 97 (1), 103–110.

Konstantatou, M., D'Acunto, P., McRobie, A., 2018. Polarities in structural analysis and design: n-dimensional graphic statics and structural transformations. Int. J. Solids Struct. 152, 272–293.

Lee, J., Van Mele, T., Block, P., 2018. Disjointed force polyhedra. Comput. Aided Des. 99, 11–28. http://dx.doi.org/10.1016/j.cad.2018.02.004.

Li, Y., Liu, Y., Xu, W., Wang, W., Guo, B., 2012. All-hex meshing using singularity-restricted field. ACM Trans. Graph. 31 (6), http://dx.doi.org/10.1145/2366145.2366196.

Liu, Y., Pottmann, H., Wallner, J., Yang, Y.-L., Wang, W., 2006. Geometric modeling with conical meshes and developable surfaces. ACM Trans. Graph. 25 (3), http://dx.doi.org/10.1145/1141911.1141941.

Maxwell, C., 1864. On reciprocal figures and diagrams of forces. London, Edinburgh, Dublin Phil. Mag. J. Sci. 27 (182), 250–261. http://dx.doi.org/10.1080/14786446408643663.

Maxwell, C., 1868. On reciprocal diagrams in space and their relation to Airy's function of stress. Proc. Lond. Math. Soc. 1 (1), 58–63.

Maxwell, C., 1870. On reciprocal figures, frames, and diagrams of forces. Earth Environ. Sci. Trans. R. Soc. Edinburgh 26 (1), 1–40.

McRobie, A., Konstantatou, M., Anthanasopoulos, G., Torpiano, G., Millar, C., Baker, W., 2021. Simple rankine gridshells. In: Proceedings of the IASS Symposium 2020/21. URL: https://www.researchgate.net/publication/358647475_Simple_Rankine_Gridshells.

McRobie, F.A., Williams, C.J.K., 2017. A stress function for 3D frames. Int. J. Solids Struct. 117, 104–110. http://dx.doi.org/10.1016/j.ijsolstr.2017.03.034.

Miki, M., Igarashi, T., Block, P., 2015. Parametric self-supporting surfaces via direct computation of Airy stress functions. ACM Trans. Graph. 34 (4), http://dx.doi.org/10.1145/2766888.

Millar, C., Mitchell, T., Mazurek, A., Chhabra, A., Beghini, A., Clelland, J.N., McRobie, A., Baker, W.F., 2021a. On designing plane-faced funicular gridshells. Manuscript submitted for publication.

Millar, C., Mitchell, T., Mazurek, A., Chhabra, A., Beghini, A., McRobie, A., Baker, W., 2021b. On funicular gridshells and airy stress functions. In: Proceedings of the IASS Symposium 2020/21. URL: https://www.researchgate.net/publication/354118428_On_funicular_gridshells_and_Airy_stress_functions.

Pellis, D., Pottmann, H., 2018. Aligning principal stress and curvature directions. In: Advances in Architectural Geometry 2018. Gothenburg, pp. 34–53, URL: https://research.chalmers.se/en/publication/504188.

Pottmann, H., Liu, Y., 2007. Discrete surfaces in isotropic geometry. In: IMA International Conference on Mathematics of Surfaces. Springer, Berlin, pp. 341–363. http://dx.doi.org/10.1007/978-3-540-73843-5_21.

Rankine, W.J.M., 1864. Principle of the equilibrium of polyhedral frames. London, Edinburgh, Dublin Phil. Mag. J. Sci. 27 (180), 92.

Timoshenko, S.P., Woinowsky-Krieger, S., 1959. Theory of Plates and Shells. McGraw-Hill.

Varignon, P., 1725. Nouvelle Mecanique ou Statique: Dont le Projet Fut DonnÉ en M. DC. LXXXVII. Jombert.

Vouga, E., Höbinger, M., Wallner, J., Pottmann, H., 2012. Design of self-supporting surfaces. ACM Trans. Graph. 31 (4), http://dx.doi.org/10.1145/2185520.2185583.

Williams, C., McRobie, A., 2016. Graphic statics using discontinuous airy stress functions. Int. J. Space Struct. 31 (2–4), 121–134. http://dx.doi.org/10.1177/0266351116660794.

Zadravec, M., Schiftner, A., Wallner, J., 2010. Designing quad-dominant meshes with planar faces. In: Computer Graphics Forum, Vol. 29. (5), Wiley Online Library, pp. 1671–1679.